

Experimental investigation of coherence contributions to a nonequilibrium thermodynamic process in a driven quantum system

Krishna Shende,^{1,*} Kavita Dorai,^{1,†} and Arvind^{1,‡}

¹*Department of Physical Sciences, Indian Institute of Science Education & Research Mohali, Sector 81 SAS Nagar, Manauli PO 140306 Punjab India.*

The work done when a system at thermal equilibrium is externally driven by a unitary control parameter leads to irreversible entropy production. The entropy produced can be thought of as a combination of coherence generation and a population mismatch between the target equilibrium state and the actually achieved final state. We experimentally explored this out-of-equilibrium process in an NMR quantum processor and studied the contribution of coherence to irreversible entropy generation. We verified a generalized Clausius inequality, which affirms that irreversible entropy production is lower-bounded.

I. INTRODUCTION

Non-equilibrium thermodynamics analyzes the behavior of systems that are far from equilibrium, either because they are undergoing rapid changes or because they are subject to external influences [1, 2]. Such non-equilibrium thermodynamics processes are usually accompanied by irreversibility and entropy production, which has been theoretically [3–6] as well as experimentally well studied on mechanical, NMR, and ion trap setups [7–11]. Quantum engines have been experimentally implemented in NMR[12, 13], superconducting qubits[14], NV centers [15] and ion traps[16, 17]. One of the key steps in constructing these quantum engines consists of driving the system from one equilibrium configuration to another, driven by an external Hamiltonian. This process is ideal when the transformation is achieved quasi-statically, but in reality this process is irreversible, which is quantified using entropy. The relative entropy produced in such a process can be divided into two parts: the first part is the contribution coming from coherence generation and other part can be attributed to the unwanted transitions occurring after the unitary transformation[5, 6]. The coherence produced is quantified using the measures proposed in Refs. [18, 19]. The Clausius inequality, $\Delta S_{irr} \geq 0$ states that the change in relative entropy is always greater than zero. In many cases, a process-specific bound is required, which can be tighter than the Clausius inequality. This type of bound for the non-equilibrium evolution of a quantum system is bounded by the Bures length between two density operators[20].

In this work we study irreversibility using an NMR quantum processor, where an NMR-active spin is initialized at thermal equilibrium and later subjected to a unitary transformation to externally drive the system into a non-equilibrium state. The driving time is changed from 100 μ s to 800 μ s, to probe the behavior of entropy

production with increasing driving time. We compute the irreversible entropy produced during this process and compare it with the theoretically expected values. We evolve the system at two different non-equilibrium states by keeping its initial equilibrium temperature same. We separate the contributions in entropy production coming from coherence generation and from unwanted transitions. We verify the inequality proposed by Bures [21], which states that entropy production is lower-bounded by a non-zero positive value.

This paper is organized as follows: In Sec.II, we briefly describe the theoretical framework of irreversible entropy and the separation of contributions from coherence and unwanted transitions. The Bures length inequality is also defined. Sec. III describes the experimental implementation in detail. Sec. IV contains a discussion of the results of the paper. A few concluding remarks are given in Sec. V.

II. THEORETICAL BACKGROUND

Recent research has focused on using coherence measures to separate the contributions to irreversible work produced in a unitary quantum process where the system is externally driven into a nonequilibrium state. The two contributions are those arising from coherence generation during the process as well as from incoherent transitions.

Assume a closed system prepared in an initial thermal equilibrium state (at inverse temperature β_i) via a Hamiltonian $H[\lambda(t)]$ with a controllable work parameter $\lambda(t)$. The system is then subjected to a Hamiltonian which changes from an initial $H_i=H[\lambda_i]$ to a final $H_f=H[\lambda_f]$, in a finite driving time τ . The initial equilibrium state is given by $\rho_i = e^{-\beta_i H_i} / Z[\lambda_i, \beta_i]$, where $Z[\lambda_i, \beta_i]$ is the partition function, β_i is the initial inverse temperature and λ_i is the work parameter. The time evolved state is given by $\rho_\tau = U_{\tau,0}[\lambda] \rho_i U_{\tau,0}^\dagger[\lambda]$, where $U_{\tau,0} = T e^{-(i/\hbar) \int_0^\tau dt H[\lambda(t)]}$ and T is the time ordering operator. Since no heat transfer takes place during this process, the irreversible work amounts to the difference between the average work ($\langle w \rangle$) and the free energy differ-

* ph19032@iisermohali.ac.in

† kavita@iisermohali.ac.in

‡ arvind@iisermohali.ac.in

ence between the initial and final equilibrium states [22]:

$$\langle w_{irr} \rangle = \langle w \rangle - \Delta F \quad (1)$$

Further, Jarzynski's relation[23] can be used to derive $\langle w \rangle \geq \Delta F$.

Consider a system initialized at $\rho_i(\beta_i, \lambda_i)$, which is driven out of equilibrium for a time τ . The actual state of the system is $\rho_\tau(\beta_\tau, \lambda_f)$ which is different from the ideal state $\rho_f(\beta_i, \lambda_f)$, as shown in Figure 1. The irreversible entropy during the transformation $\rho_i \rightarrow \rho_\tau$ is defined as [3]:

$$\Delta S_{irr} = \beta_i \langle w_{irr} \rangle = \beta_i (\langle w \rangle - \Delta F) = D(\rho_\tau || \rho_f) \quad (2)$$

where $D(\rho_\tau || \rho_f)$ is the quantum relative entropy[24] between the actual density operator ρ_τ and the equilibrium density operator. The non-equilibrium lag in Eqn. 2 is a 'proxy' for entropy production, since, after the driving when the system is coupled to the bath, it will relax from ρ_τ to ρ_f [6, 25, 26].

The irreversible entropy can be decomposed into two parts: (1) unwanted transitions occurring between energy levels during the external driving which makes the populations between ρ_τ and ρ_f distinct, and (2) the coherence generated in the actual state ρ_τ [5]:

$$\Delta S_{irr} = C(\rho_\tau) + D(\Delta_\tau[\rho_\tau] || \rho_B) \quad (3)$$

where the contribution due to coherence generation is quantified using the relative entropy of coherence of ρ_τ given by [18, 19]:

$$C(\rho_\tau) = D(\rho_\tau || \Delta_\tau[\rho_\tau]) = S(\Delta_\tau[\rho_\tau]) - S(\rho_\tau). \quad (4)$$

By construction, both the coherence and the mismatch in the population difference between actual and final equilibrium states are positive, hence the increase in either of these quantities leads to an increase in total entropy production.

The Clausius inequality, $\Delta S_{irr} \geq 0$, provides a fundamental bound on irreversible entropy production for a nonequilibrium thermodynamic process, which is independent of how far from equilibrium the system reaches after the process. Using a geometric approach for classical cases near equilibrium, the entropy produced is given by the Riemannian distance between the initial and final states is given by [27–31]:

$$dS_{irr} \geq dl^2/2 \quad (5)$$

where the thermodynamic length (l) has been shown to be the same as Wootters' statistical distance between two pure states ρ_τ and ρ_f , given by [32]:

$$l(p_\tau, p_f) = \arccos \left(\int dx \sqrt{p_\tau(x)p_f(x)} \right) \quad (6)$$

where p_i and p_τ are the probability distributions of ρ_0 and ρ_τ .

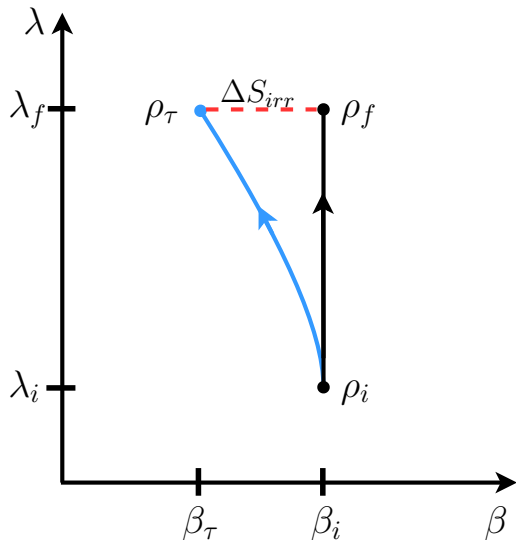


FIG. 1. (Color online) Schematic diagram of a non-equilibrium quantum thermodynamic process, with the system Hamiltonian $H[\lambda(t)]$ initially prepared in an equilibrium state $\rho_i(\beta_i, \lambda_i)$ at $\tau=0$. The system is then pushed out of equilibrium by changing the parameter $\lambda(t)$ to λ_f during a time τ . The irreversible entropy produced during this process is due to the work difference between the actual state of the system ρ_τ and the final equilibrium state $\rho_f(\beta_i, \lambda_f)$.

The Clausius inequality has been generalized to quantum nonequilibrium processes by Deffner et.al [3], which also places a lower bound on the amount of entropy produced and is given by:

$$\Delta S_{irr} \geq \frac{8}{\pi^2} L^2(\rho_\tau, \rho_f) \quad (7)$$

where L is the finite Bures length, which is a quantum generalization of the thermodynamic length and for two density operators, is given by [27–29, 31]:

$$L(\rho_1, \rho_2) = \arccos \sqrt{F(\rho_1, \rho_2)} \quad (8)$$

where F is the fidelity between two quantum states and is given by [33, 34]:

$$F(\rho_1, \rho_2) = \left[\text{Tr} \left(\sqrt{\sqrt{\rho_1} \rho_2 \sqrt{\rho_1}} \right) \right]^2 \quad (9)$$

It is evident from Eqn. 7 that quantum entropy production ΔS_{irr} is bounded from below by the geometric distance between the actual density operator and the equilibrium density operator. The further the system is from equilibrium, the more is the entropy produced.

III. EXPERIMENTAL IMPLEMENTATION

An NMR quantum processor consists of an ensemble of nuclear spins isotropically tumbling in a large static

magnetic field, from which qubits (spin-1/2 nuclei) can be realized. In the high-temperature, high-field approximation, NMR qubits follow a Boltzmann population distribution, which gives rise to a net magnetization along the z -direction (parallel to the applied magnetic field). The NMR Hamiltonian for a two-qubit system in the rotating frame is given by [35]:

$$\mathcal{H} = -\hbar \sum_{i=1}^2 \omega_i I_z^i + \hbar \sum_{i<j=1}^2 J_{ij} I_z^i I_z^j \quad (10)$$

where ω_i the offset frequency of the i^{th} nucleus, I_z^i represents the z -component of the spin angular momentum of the i^{th} nucleus and J_{ij} is the scalar coupling between the i^{th} and the j^{th} nuclei.

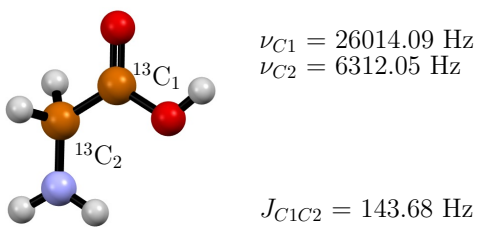


FIG. 2. (Color online) Molecular structure of ^{13}C -labeled glycine with the $^{13}\text{C}_1$ and $^{13}\text{C}_2$ spins encoded as the first and second qubit, respectively. The offset rotation frequency for each spin and scalar coupling strengths are listed alongside.

The molecule of ^{13}C -labeled glycine has been used to realize a system of two NMR qubits (Figure 2). The quantum circuit and corresponding pulse sequence to perform the study of non-equilibrium dynamics is shown in Figure 3. The spatial averaging technique[36] has been used to initialize the system in the pseudopure state $|00\rangle\langle 00|$, with the corresponding density operator given by

$$\rho_{00} = \frac{1 - \epsilon}{4} I_4 + \epsilon |00\rangle\langle 00| \quad (11)$$

where I_4 is the 4×4 identity operator and ϵ is proportional to the spin polarization ($\approx 10^{-5}$ at room temperature). The circuit and pulse sequence used to achieve this is shown in the blue shaded portion of Figure 3. Starting from this pseudopure state, the qubits were initialized in the Gibbs thermal state with the inverse temperature β_i achieved by applying an rf pulse with an angle of rotation between 0 and $\frac{\pi}{2}$, which redistributes the population between the qubit states and also creates coherences. To achieve the final thermal state, wherein each spin is equilibrated at a different pseudospin temperature, pulsed field gradient (PFG) pulses were applied to kill the unwanted off-diagonal elements of the density matrix. Quantum state tomography was performed to compute the state fidelity and to verify that the system has been initialized to the required Gibbs state. Gradient

ascent pulse engineering (GRAPE) [37], an optimal control technique, was used to generate high-fidelity rf pulses of duration $\approx 150\mu\text{ s}$ to implement single-qubit unitary rotations. Pulses generated using GRAPE were also used to drive the system out of equilibrium, which are shown in the yellow shaded section of Figure 3. All experiments were performed at room temperature on a Bruker Avance III 600-MHz FT-NMR spectrometer equipped with a QXI probe.

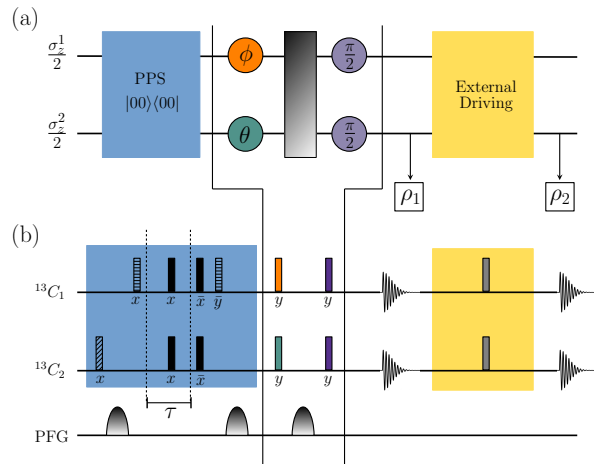


FIG. 3. (Color online) (a) Circuit diagram to realize a non-equilibrium quantum thermodynamic process on an NMR processor. The circuit to achieve the pseudopure state (PPS) $|00\rangle\langle 00|$ as shown in the shaded blue box. Orange and teal circles represent unitary gates with angle of rotation fixed at ϕ and θ respectively, which controls the equilibrium spin temperature of each qubit. The shaded yellow box depicts the external driving circuit which drives the system out of equilibrium. (b) NMR pulse sequence to implement the circuit given in panel (a). Cross-hatched lined, horizontal lined and filled rectangles represent rf pulses of $\frac{\pi}{3}$, $\frac{\pi}{4}$ and π rotation angle respectively, with their respective rotation axes given below each shaded rectangle. Orange, teal and indigo rectangles represent rf pulses of ϕ , θ and $\frac{\pi}{2}$ rotation angles respectively, applied along the y -axis. Grey shaded rectangles correspond to external driving unitary pulses. The PFG line depicts the times at which a gradient is employed to destroy coherence. The time delay τ is set equal to $\frac{1}{2J_{C1C2}}$.

The effective spin temperature (β_i) of the initial Gibbs state is related to the ground (p_0) and excited (p_1) populations by:

$$\beta_i = \frac{1}{h\nu} \ln \left(\frac{p_0}{p_1} \right) \quad (12)$$

where h is Planck's constant and ν is the offset frequency. After creation of the pseudopure state, the population exchange between the ground and excited states can be controlled by applying an appropriate rf pulse, or initialize the system to the desired Gibbs state. Both the spins were initialized to an initial temperature of $(\beta_i h)^{-1} = 1580.2 \text{ Hz}$, where the initial energy gap (ν) was set to 2000 Hz.

The Hamiltonian which was used to drive the system out of equilibrium is given by [9, 12, 13]:

$$H(\nu(t)) = -\frac{1}{2}h\nu(t)[\cos(\pi t/2\tau)\sigma_x + \sin(\pi t/2\tau)\sigma_y] \quad (13)$$

where $\nu(t) = \nu_i(1 - (t/\tau)) + \nu_f(t/\tau)$. The energy gap can be expanded from ν_i at time $t = 0$ to ν_f at $t = \tau$ via implementation of the unitary ($U_{\tau,0}$) calculated as [13]:

$$U_{\tau,0} = \exp\left(-i/\hbar \int_0^\tau H(\nu(t))dt\right). \quad (14)$$

Non-equilibrium dynamics was probed by keeping the initial energy gap ν_i fixed at 2000 Hz and setting the ν_f to two different values, namely, 3600 Hz and 5000 Hz, respectively. The driving time to drive the system into a nonequilibrium state is varied from 100 μs to 800 μs . This driving time is much less than the decoherence times of the system qubits, and hence the process can be considered to be almost unitary.

Quantum state tomography [38, 39] was performed to confirm the closeness between the experimental and theoretical state and to calculate irreversible work and coherence. The density matrix corresponding to an initial equilibrium state (ρ_i) and to a final non-equilibrium state (ρ_f) was reconstructed. The similarity between the theoretically predicted density operator (ρ_t) and the experimentally reconstructed density operator (ρ_e) is given by the fidelity [40]:

$$F = \frac{|Tr(\rho_e\rho_t^\dagger)|}{\sqrt{Tr(\rho_e\rho_e^\dagger)Tr(\rho_t\rho_t^\dagger)}} \quad (15)$$

The high experimental fidelities validate the good match between the theoretically expected and the experimentally obtained values of irreversible work and coherence.

IV. RESULTS AND DISCUSSION

Experiments were performed by first initializing the spin temperature of both the ^{13}C qubits to $(\beta_i\hbar)^{-1}=1580.2$ Hz at thermal equilibrium. In order to probe system dynamics, it was driven out of equilibrium, on a time scale varying from 100 μs to 800 μs . During the driving process, the initial energy gap was fixed at 2000 Hz and then changed to 3600 Hz; this process was repeated with the final energy gap changed from 2000 Hz to 5000 Hz. The final energy gap indicates how far the system is driven from equilibrium; the larger the gap, the further the system moves away from equilibrium.

The behavior of various quantities are plotted in Figure 4 and Figure 5 for a final energy gap of 3600 Hz and 5000 Hz, respectively. The irreversible entropy (ΔS_{irr}), coherence ($C(\rho(\tau))$) and $8/\pi^2$ times the square of the Bures length ($8L^2/\pi^2$) are plotted in Figures 4 and 5, as a function of the system driving time. It is evident from the plots that for low driving times, the system produces

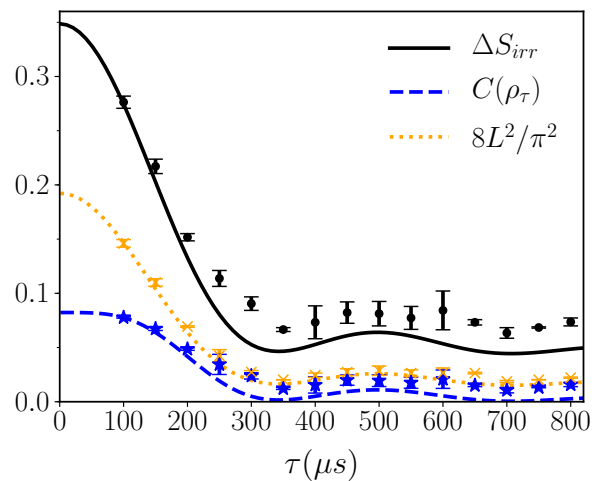


FIG. 4. (Color online) Dynamics of entropy (ΔS_{irr}), coherence ($C(\rho(\tau))$), and the lower bound on entropy ($8L^2/\pi^2$), plotted as a function of driving time (τ). The energy gap is varied from 2000 Hz to 3600 Hz. Theoretical predictions are plotted as solid curves, while experimental data (with error bars) are plotted as circles, stars and crosses, respectively.

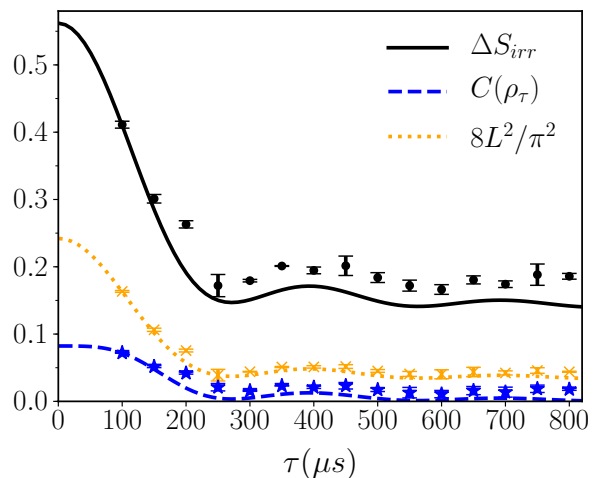


FIG. 5. (Color online) Same as Figure 4, but with the energy gap varied from 2000 Hz to 5000 Hz.

more entropy, since the driving time is far away from the ideal quasi-static change in the system. As the driving time is increased, the irreversible entropy production gradually decreases, since the process is approaching a quasi-static process. The coherence production follows the same trend as the irreversible entropy production.

The contribution of coherence to irreversible entropy production is more for a final energy gap of 3600 Hz as compared to 5000 Hz. This is evident from the fact that the gap between the coherence curve and irreversible entropy curve is less in the plot depicted in Figure 4 as compared to the plot depicted in Figure 5. The irreversible entropy produced is more for a final energy gap of 5000 Hz (Figure 4) as compared to a final energy gap

of 3600 Hz (Figure 5), since the system is driven further away from equilibrium for higher final energy gaps. As the driving time is increased, the contribution due to coherence is almost negligible and the population difference between the states is the major factor determining the irreversible entropy production. Hence, we are able to separate the irreversible entropy generated due to coherence production and the mismatch in the population difference between the actual state and the equilibrium state. We have explored the validity of the inequality given in Eqn. 7 in Figures 4 and 5 for a final energy gap of 3600 Hz and 5000 Hz, respectively. It can be observed that the inequality is always satisfied, which implies that the irreversible entropy production is lower bounded. Discrepancies between the theoretical curves and the experimental data can be attributed to errors in pulse calibration, initial state preparation, magnetic field inhomogeneities, and GRAPE pulse optimization. These errors lead to a final state being slightly different than the theoretical expected state, which leads to the production of extra entropy. Hence the experimental data points are slightly above the theoretical curve (Figures 4 and 5).

V. CONCLUSIONS

We have experimentally investigated an out-of-equilibrium quantum thermodynamic process, where a system at thermal equilibrium is subjected to an exter-

nal driving force, which results in the production of entropy. This irreversible entropy has two separate contributions, one due to coherence generation after external driving and the other due to a population mismatch between the actual state and the equilibrium state. We performed experiments by keeping the spin temperature of the spins fixed and then driving the energy gap from an initial 2000 Hz to 3600 Hz and later upto a frequency of 5000 Hz. We found that coherence generation follows the irreversible entropy trend, in that the amount of entropy generated increases with increasing energy gap, and concomitantly, the contribution to entropy generation due to coherence is decreased. We also verified the validity of a generalized Clausius inequality, which states that the irreversible entropy production is lower-bounded by the Bures length between the actual state and the equilibrium state. We were able to time-separate the contribution of coherence to entropy generation and also verified that the irreversible entropy generation is lower bounded for a non-equilibrium process which is externally driven.

ACKNOWLEDGMENTS

All experiments were performed on a Bruker Avance-III 600 MHz FT-NMR spectrometer at the NMR Research Facility at IISER Mohali. K.S. acknowledges financial support from the Prime Minister's Research Fellowship (PMRF) scheme of the Government of India.

-
- [1] R. Kawai, J. M. R. Parrondo, and C. V. den Broeck, *Phys. Rev. Lett.* **98**, 080602 (2007).
 - [2] J. M. R. Parrondo, C. V. den Broeck, and R. Kawai, *New Journal of Physics* **11**, 073008 (2009).
 - [3] S. Deffner and E. Lutz, *Phys. Rev. Lett.* **105**, 170402 (2010).
 - [4] F. Plastina, A. Alecce, T. J. G. Apollaro, G. Falcone, G. Francica, F. Galve, N. Lo Gullo, and R. Zambrini, *Phys. Rev. Lett.* **113**, 260601 (2014).
 - [5] G. Francica, J. Goold, and F. Plastina, *Phys. Rev. E* **99**, 042105 (2019).
 - [6] J. P. Santos, L. C. Céleri, G. T. Landi, and M. Paternostro, *npj Quantum Information* **5**, 23 (2019).
 - [7] J. V. Koski, T. Sagawa, O.-P. Saira, Y. Yoon, A. Kutvonen, P. Solinas, M. Möttönen, T. Ala-Nissila, and J. P. Pekola, *Nature Physics* **9**, 644 (2013).
 - [8] T. B. Batalhão, A. M. Souza, L. Mazzola, R. Auccaise, R. S. Sarthour, I. S. Oliveira, J. Goold, G. De Chiara, M. Paternostro, and R. M. Serra, *Phys. Rev. Lett.* **113**, 140601 (2014).
 - [9] T. B. Batalhão, A. M. Souza, R. S. Sarthour, I. S. Oliveira, M. Paternostro, E. Lutz, and R. M. Serra, *Phys. Rev. Lett.* **115**, 190601 (2015).
 - [10] S. An, J.-N. Zhang, M. Um, D. Lv, Y. Lu, J. Zhang, Z.-Q. Yin, H. T. Quan, and K. Kim, *Nature Physics* **11**, 193 (2015).
 - [11] A. Smith, Y. Lu, S. An, X. Zhang, J.-N. Zhang, Z. Gong, H. T. Quan, C. Jarzynski, and K. Kim, *New Journal of Physics* **20**, 013008 (2018).
 - [12] J. P. S. Peterson, T. B. Batalhão, M. Herrera, A. M. Souza, R. S. Sarthour, I. S. Oliveira, and R. M. Serra, *Phys. Rev. Lett.* **123**, 240601 (2019).
 - [13] R. J. de Assis, T. M. de Mendonça, C. J. Villas-Boas, A. M. de Souza, R. S. Sarthour, I. S. Oliveira, and N. G. de Almeida, *Phys. Rev. Lett.* **122**, 240602 (2019).
 - [14] A. Solfanelli, A. Santini, and M. Campisi, *PRX Quantum* **2**, 030353 (2021).
 - [15] J. Klatzow, J. N. Becker, P. M. Ledingham, C. Weinzetl, K. T. Kaczmarek, D. J. Saunders, J. Nunn, I. A. Walmsley, R. Uzdin, and E. Poem, *Phys. Rev. Lett.* **122**, 110601 (2019).
 - [16] J. Roßnagel, S. T. Dawkins, K. N. Tolazzi, O. Abah, E. Lutz, F. Schmidt-Kaler, and K. Singer, *Science* **352**, 325 (2016).
 - [17] G. Maslennikov, S. Ding, R. Hablützel, J. Gan, A. Roulet, S. Nimmrichter, J. Dai, V. Scarani, and D. Matsukevich, *Nature Communications* **10**, 202 (2019).
 - [18] T. Baumgratz, M. Cramer, and M. B. Plenio, *Phys. Rev. Lett.* **113**, 140401 (2014).
 - [19] A. Streltsov, G. Adesso, and M. B. Plenio, *Rev. Mod. Phys.* **89**, 041003 (2017).
 - [20] S. Kakutani, *Annals of Mathematics* **49**, 214 (1948).

- [21] S. L. Braunstein and C. M. Caves, *Phys. Rev. Lett.* **72**, 3439 (1994).
- [22] S. Deffner and S. Campbell, *Quantum Thermodynamics*, 2053-2571 (Morgan & Claypool Publishers, 2019).
- [23] C. Jarzynski, *Phys. Rev. Lett.* **78**, 2690 (1997).
- [24] H. Umegaki, *Kodai Mathematical Seminar Reports* **14**, 59 (1962).
- [25] H. Spohn and J. L. Lebowitz, “Irreversible thermodynamics for quantum systems weakly coupled to thermal reservoirs,” in *Advances in Chemical Physics* (1978) pp. 109–142.
- [26] H.-P. Breuer, *Phys. Rev. A* **68**, 032105 (2003).
- [27] P. Salamon and R. S. Berry, *Phys. Rev. Lett.* **51**, 1127 (1983).
- [28] P. Salamon, J. D. Nulton, and R. S. Berry, *The Journal of Chemical Physics* **82**, 2433 (1985).
- [29] J. Nulton, P. Salamon, B. Andresen, and Q. Anmin, *The Journal of Chemical Physics* **83**, 334 (1985).
- [30] G. Ruppeiner, *Rev. Mod. Phys.* **67**, 605 (1995).
- [31] G. E. Crooks, *Phys. Rev. Lett.* **99**, 100602 (2007).
- [32] W. K. Wootters, *Phys. Rev. D* **23**, 357 (1981).
- [33] A. Uhlmann, *Reports on Mathematical Physics* **9**, 273 (1976).
- [34] R. Jozsa, *Journal of Modern Optics* **41**, 2315 (1994).
- [35] I. S. Oliveira, T. J. Bonagamba, R. S. Sarthour, J. C. Freitas, and E. R. deAzevedo, in *NMR Quantum Information Processing*, edited by I. S. Oliveira, T. J. Bonagamba, R. S. Sarthour, J. C. Freitas, and E. R. deAzevedo (Elsevier Science B.V., Amsterdam, 2007) pp. 137–181.
- [36] D. G. Cory, M. D. Price, and T. F. Havel, *Physica D: Nonlinear Phenomena* **120**, 82 (1998), proceedings of the Fourth Workshop on Physics and Consumption.
- [37] N. Khaneja, T. Reiss, C. Kehlet, T. Schulte-Herbrüggen, and S. J. Glaser, *Journal of Magnetic Resonance* **172**, 296 (2005).
- [38] A. Gaikwad, Arvind, and K. Dorai, *Quantum Information Processing* **20**, 19 (2021).
- [39] A. Gaikwad, Arvind, and K. Dorai, *Quantum Information Processing* **21**, 388 (2022).
- [40] J. Zhang, A. M. Souza, F. D. Brandao, and D. Suter, *Phys. Rev. Lett.* **112**, 050502 (2014).